Journal of ELECTRONIC MATERIALS, Vol. 41, No. 11, 2012
DOI: 10.1007/s11664-012-2193-4


# Crystal Structure of Cu-Sn-In Alloys Around the $\eta$-Phase Field Studied by Neutron Diffraction

G. AURELIO,[1,4] S.A. SOMMADOSSI,[2] and G.J. CUELLO[3]

1.—Consejo Nacional de Investigaciones Científicas y Técnicas, Centro Atómico Bariloche, Comisión Nacional de Energía Atómica, Av. Bustillo 9500, S. C. de Bariloche, RN 8400, Argentina. 2.—IDEPA, Consejo Nacional de Investigaciones Científicas y Técnicas, Facultad de Ingeniería, Universidad Nacional del Comahue, 8300 Buenos Aires 1400, Neuquén, Argentina. 3.—Institut Laue Langevin, Grenoble 38042, France. 4.—e-mail: gaurelio@cab.cnea.gov.ar

Study of the Cu-Sn-In ternary system has become quite important in recent years, due to new environmental regulations increasingly restricting use of Pb for bonding technologies in electronic devices. A key relevant issue concerns the intermetallic phases which grow in the bonding zone and strongly affect its quality and performance. In this work, we focus on the $\eta$-phase ($Cu_2In$ or $Cu_6Sn_5$) that exists in both end binaries and as a ternary phase. We present a neutron diffraction study of the constitution and crystallography of a series of alloys around the 60 at.% Cu composition, and with In contents ranging from 0 at.% to 25 at.%, quenched from 300°C. The alloys were characterized by scanning electron microscopy (SEM), electron probe microanalysis (EPMA), and high-resolution neutron diffraction (ND). Rietveld refinement of ND data allowed improvement of the currently available model for site occupancies in the hexagonal $\eta$-phase in the binary Cu-Sn as well as in ternary alloys. For the first time, structural data are reported for the ternary Cu-Sn-In $\eta$-phase as a function of composition, information that is of fundamental technological importance as well as valuable for ongoing modeling of the ternary phase diagram.

**Key words:** Pb-free solders, Cu-Sn alloys, neutron diffraction

## INTRODUCTION

Since the recent emergence of environmental regulations increasingly restricting use of Pb in soldering and bonding technologies in the electronics industry, study of Pb-free alternative alloys has received major attention.[1] Not only new materials but also new soldering methods are being explored to improve the performance of joints under high-temperature working conditions, such as so-called transient liquid-phase bonding (TLPB) or diffusion soldering.[2] This method relies on a diffusion–reaction process between an interlayer solder and the parent material or substrate, which in the electronics industry is mostly copper. The advantage of TLPB lies in the production of joints with microstructures and mechanical properties very similar to those of the parent material, and capable of withstanding higher temperatures.

Sn-based alloys are among the favorite Pb-alloy substitutes for use in bonding technology, having low melting points, low cost, good wettability, etc. In particular, the Sn-In binary system with its eutectic point at only 120°C (In-48 at.% Sn) constitutes an excellent candidate to lower the processing temperature of joints. However, interfacial reactions at the solder/Cu interface and in the solder matrix lead to the formation of intermetallic phases (IPs) which are often brittle and hard, causing solder joint failure. Therefore, if Sn-In alloys are to become solder candidates, the properties of the ternary Cu-Sn-In system and its IPs as constituents of microelectronic solder joints become a fundamental matter of research. Paradoxically, the equilibrium phase diagram of the Cu-Sn-In system is still not completely

(Received April 9, 2012; accepted June 29, 2012; published online August 2, 2012)

determined. It remains under evaluation,[3] with a few experimental studies[4–6] and one complete thermodynamic calculation using CALPHAD.[7] However, even the binaries Cu-Sn and Cu-In present discrepancies regarding the crystallography of the numerous IPs.

Of particular interest for industry and TLPB technology is the IP called $\eta$-phase, which is present in both Cu-In ($Cu_2In$) and Cu-Sn ($Cu_6Sn_5$) alloys, as it is commonly found in the Cu/solder interface. This phase presents polymorphic transitions with temperature, so in order to avoid confusion between the two binaries, in the present work the high-temperature form is called $\eta$(HT) and the low-temperature modification is called $\eta$(LT). For $Cu_6Sn_5$ the $\eta(HT) \rightarrow \eta(LT)$ transition occurs at 186°C, whereas for $Cu_2In$ it would occur between 306°C and 383°C for some authors,[8,9] while for others the sequence of phases is more complex.[10,11] In Cu-Sn alloys, the LT → HT transition is accompanied by a specific volume change of about 2.15% which is highly disadvantageous for the performance of soldered joints as it produces cracks.[12,13]

Despite the unclear scenario regarding the crystallography and stability of $Cu_2In$ alloys, it has been proposed that $Cu_2In$ and $Cu_6Sn_5$ form a continuous solid solution in the ternary phase diagram between 186°C and 383°C, but no further details are given about the ternary $\eta$-phase. It is important to note that the proposal of a continuous solid solution comes from microscopy observations of microstructure and by conventional x-ray diffraction (XRD) which cannot yield any information on the atomic distribution of In and Sn in the proposed hexagonal crystallographic cell, as the two elements are neighbors in the Periodic Table. We present in this paper the first neutron powder diffraction (ND) study of ternary Cu-Sn-In alloys focusing on the crystal structure and phase stability of the $\eta$-phase. Previous works and our experience indicate that, unless very carefully prepared, powders of these alloys are difficult to study using x-ray diffraction methods. This is mainly due to a large linear absorption coefficient for Cu $K_\alpha$ radiation, and severe preferred orientation,[14] in particular for alloys subjected to long aging treatments. By using ND we have largely overcome these issues. The objective of the present work is to present a systematic study of the crystallography of the $\eta$-phase in ternary Cu-In-Sn alloys, tracking the atomic arrangement as the composition is varied from the binary Cu-Sn $\eta$-phase towards the binary Cu-In $\eta$-phase in the 300°C isothermal section.

## EXPERIMENTAL PROCEDURES

### Alloys

Seven Cu-In-Sn alloys with nominal compositions lying in the proximity of the $\eta$-phase field are discussed in this paper. The alloys were prepared by melting nominal amounts of the high-purity (4 N) elements in an electric furnace under a reducing Ar atmosphere, and then cooling in air. The resulting ingots were encapsulated in quartz ampoules under Ar atmosphere, annealed at 300°C for 3 weeks to promote homogenization, and then rapidly quenched to 0°C.

Optical microscopy inspection of Sn-rich alloys S1–S5 reveals a microstructure composed of well-developed grains with average size of 300 $\mu$m (matrix), some Sn segregation at grain boundaries, and small amounts of a second phase close to the edges with a different morphology, which tend to disappear with increasing In content. We discuss this issue further in "Results" section.

The composition of the alloys was determined by electron probe microanalysis (EPMA) using the wavelength-dispersive spectroscopy (WDS) technique under an acceleration voltage of 15 kV. Measurements were performed on several spots corresponding to the matrix, grain boundaries, and segregated phase. Results are summarized in Table I. Based on the phase diagrams available for these alloys,[15] the matrix would correspond to the $\eta$-phase and the

**Table I. Composition of the Cu-In-Sn alloys studied in the present work**

| | Nominal at.% | | | Matrix at.% | | | Segregated at.% | | | Grain Boundaries at.% | | |
|---|---|---|---|---|---|---|---|---|---|---|---|---|
| **Sample** | **Cu** | **In** | **Sn** | **Cu** | **In** | **Sn** | **Cu** | **In** | **Sn** | **Cu** | **In** | **Sn** |
| S1 | 55 | 0 | 45 | 53.9 | | 46.0 | 73.8 | 0.0 | 26.1 | 3.0 | 0.2 | 96.8 |
| S2 | 55 | 1 | 44 | 54.3 | 1.1 | 44.5 | 74.2 | 0.2 | 25.6 | 2.1 | 2.1 | 95.8 |
| S3 | 55 | 3 | 42 | 53.9 | 3.1 | 43.0 | 73.7 | 0.6 | 25.6 | 2.02 | 6.07 | 91.9 |
| S4 | 55 | 5 | 40 | 55.6 | 5.0 | 39.4 | 74.0 | 1.1 | 24.9 | 0.9 | 57.2 | 87.7 |
| S5 | 58 | 12 | 30 | 58.1 | 12.2 | 29.7 | 74.2 | 3.2 | 22.6 | – | – | – |
| S6 | 60 | 20 | 20 | 61.2 | 20.4 | 18.4 | – | – | – | – | – | – |
| S7 | 60 | 24 | 16 | 60.8* | 24.5* | 14.7* | – | – | – | – | – | – |

Samples S1–S6 were measured by WDS, selecting grains from the middle and from each edge of the ingots. The global composition of sample S7 (marked with *) was measured by energy-dispersive spectroscopy (EDS).

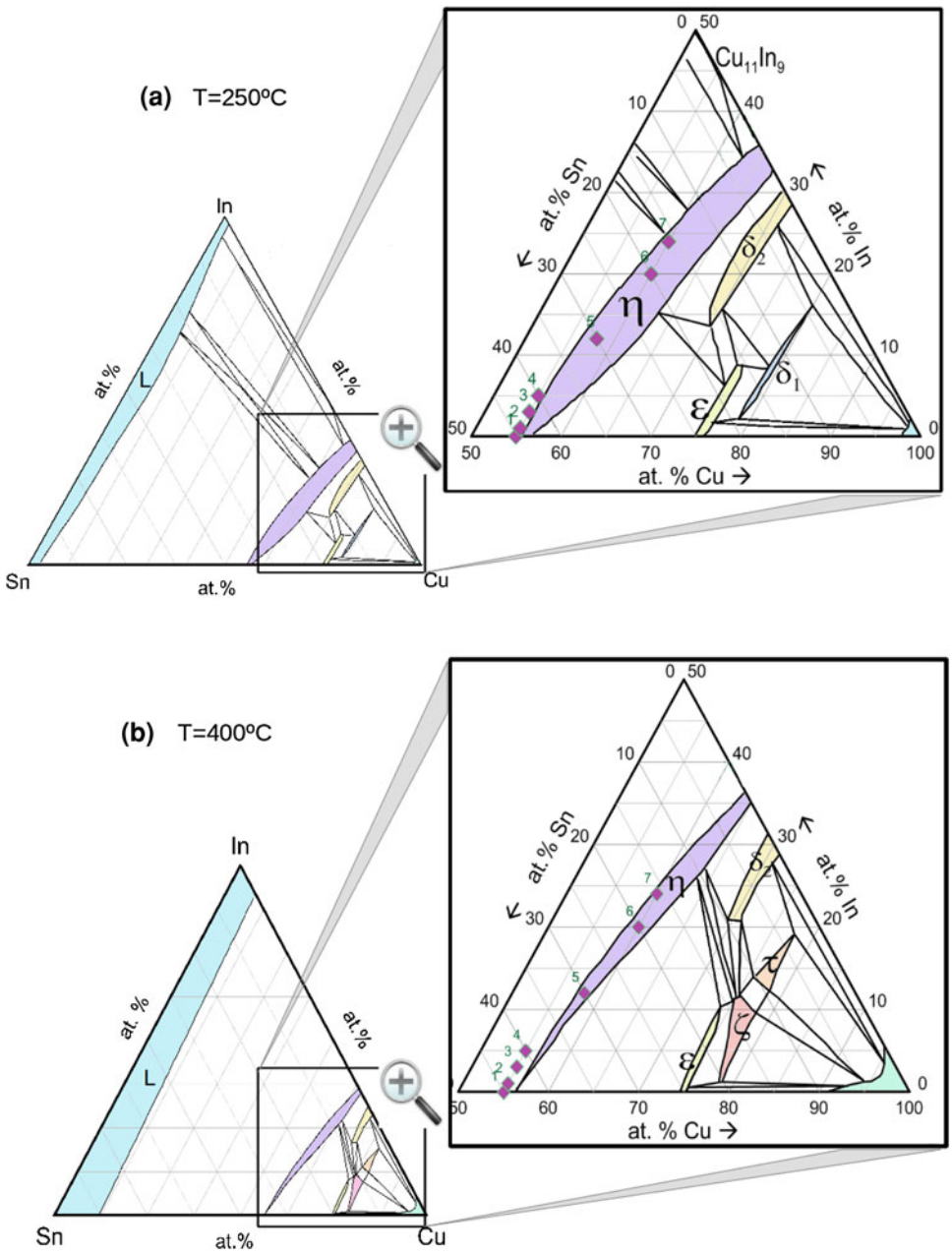


Fig. 1. Isothermal sections of the Sn-In-Cu ternary system at (a) 250°C after Lin et al.[6] and (b) 400°C after Köester et al.[4] Symbols denote the alloys studied in the present work, while shaded areas correspond to the following phase fields: $\eta$ : $Cu_6Sn_5$, $Cu_2In$; $\varepsilon$ : $Cu_3Sn$; $\delta_1$ : $Cu_{41}Sn_{11}$; $\delta_2$ : $Cu_7In_3$; $\zeta$ : $Cu_{10}Sn_3$; $\tau$ : $Cu_{11}In_2Sn$[4] or $Cu_{16}In_3Sn$.[7]

segregated striped phase to the $\varepsilon$-phase $Cu_3Sn$, in agreement with microanalysis results.

In Fig. 1 we present the two currently available isothermal sections of the ternary phase diagram closest to the annealing temperature used in the present work: at 250°C[6] and at 400°C.[4] Superimposed on the diagrams we indicate the nominal composition of our alloys, labelled S1–S7.

## Neutron Diffraction

High-resolution ND experiments were performed at the Institut Laue-Langevin (ILL) in Grenoble, France. ND data at room temperature were collected at diffractometer Super-D2B. A wavelength of ~1.59 Å was used, with angular span of 150° and step of 0.05°. The collimated beam on the sample was 32 mm × 9 mm using 50-mm horizontal slits. A Si standard was used to calibrate the neutron wavelength, yielding the value $\lambda = 1.5937 \pm 0.0002$ Å. This was in very good agreement with the calibration performed by the beamline staff using a NaCaAlF standard ($\lambda = 1.5935$ Å).

Samples for ND experiments were obtained by manually grinding alloy ingots for 10 min in an agate mortar, resulting in fine powder. Measurements were

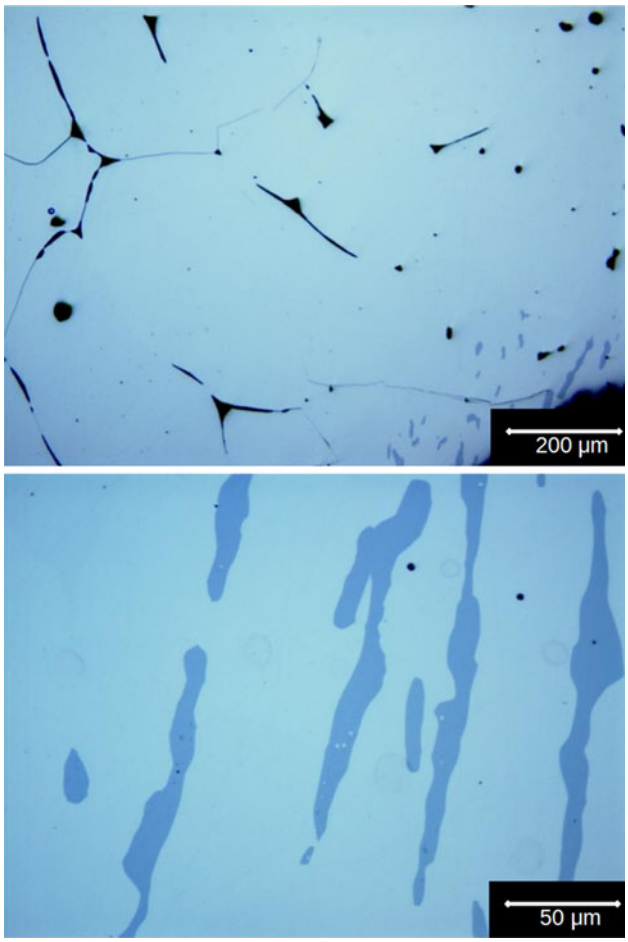


Fig. 2. Optical micrographs for sample S1 at different magnifications.

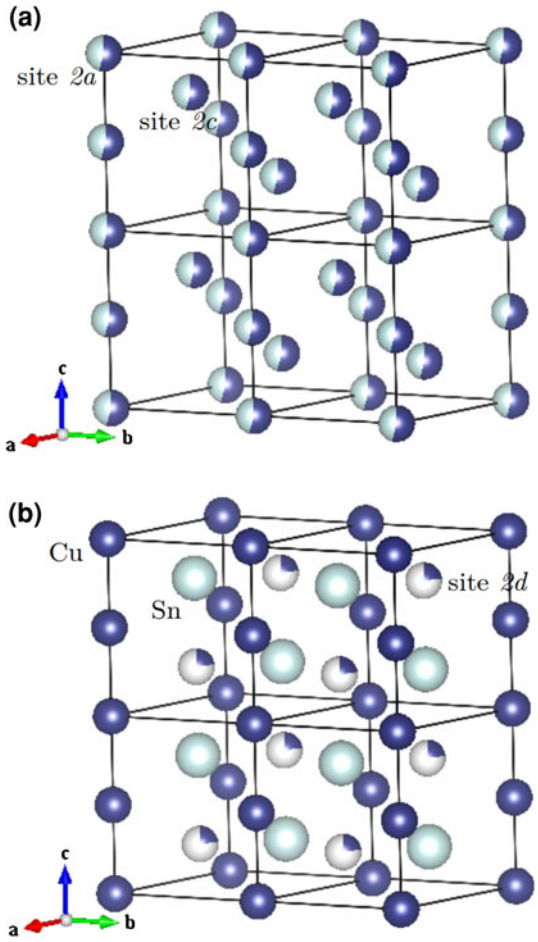


Fig. 3. (a) Crystallographic model currently available for the high-temperature $Cu_6Sn_5$ phase (ICSD 56282) in which Cu (dark atoms) and Sn (light atoms) occupy randomly the Wykoff sites *2a* and *2c*, represented by partial shadings. Solid lines indicate the unit cells (four in the picture) of the $P6_3/mmc$ space group. (b) Crystallographic model resulting from refinement of ND data. Cu atoms occupy completely site *2a* and In atoms site *2c*. The remaining Cu partially occupies site *2d*. Figure produced using the software VESTA.[21]

performed in vanadium cylinders of 6 mm diameter and 8 cm height filled with sample. Patterns were collected in 150 min, and the diffractograms thus obtained were processed with the full-pattern analysis Rietveld method, using the program FULLPROF.[16]

## RESULTS

### Constitution of the Alloys

Optical micrographs of sample S1 at different magnifications are presented in Fig. 2. These images show the presence of a main homogeneous matrix, a segregated phase with a striped morphology, and some material at the grain boundaries. EPMA measurements collected at each of these regions (Table I) reveal that the matrix corresponds to the $Cu_6Sn_5$ ($\eta$) composition, the segregated phase corresponds to the $Cu_3Sn$ ($\varepsilon$) composition, and that some pure Sn is present at the grain boundaries. The high-resolution ND data for this sample confirm the coexistence of the $\eta$- and $\varepsilon$-phases, but no traces were found of the crystalline $\beta$-Sn phase, suggesting that the quenching process resulted in retention of noncrystalline Sn from the melt. This is also supported by the background profile in the diffractograms. Diffraction from the $\eta$- and $\varepsilon$-phases show, on the other hand, a high degree of crystallinity.

The refinement strategy started with the available model for the high-temperature $Cu_6Sn_5$ phase (ICSD 56282, after Ref. 17) in which Cu and Sn atoms occupy randomly the Wykoff positions *2a* and *2c* of the $P6_3/mmc$ space group; i.e., the occupancy of each site is 55% Cu and 45% Sn, as schematized in Fig. 3a. Although the cell metrics were correct, this model could not account for the relative intensities in our diffractogram and led to poor fits, as shown in Fig. 4a. Refinements improved greatly (Fig. 4b) when site occupancies were set to *2a* with 100% Cu and *2c* with 100% Sn. The excess Cu was allowed to occupy the *2d* site as in the high-temperature $Cu_2In$ $\eta$-phase (ICSD 102982 after Ref. 18, ICSD 627998 after Ref. 19). All attempts to refine these occupancies with both

atom types quickly converged to the same result, schematized in Fig. 3b. In fact, this distribution of atoms is the one that actually corresponds to NiAs, as also used to refine the XRD data of $Cu_6Sn_5$ by Nogita et al.[20] as well as Peplinski et al.[14]

On the other hand, several models are available in the literature for the $\varepsilon$-phase $Cu_3Sn$, such as ICSD cards 162569, 103102, 103103, and 629268. Among them, our ND data could only be successfully refined using the orthorhombic space group *Cmcm* with a long-period superlattice (ICSD 103102 and PDF 65-5721 after Ref. 22). This has been previously reported to be the case when samples are annealed for a long time in the high-temperature $\varepsilon$-phase region and subsequently quenched.[23] As this phase is only found in samples with very little In, the refinements were performed considering stoichiometric $Cu_3Sn$ to simplify the problem, although according to the available phase diagrams, this phase should present a certain In solubility too. In Fig. 5 we show the complete Rietveld refinement (solid line) of the high-resolution data (symbols) collected at room temperature for sample S1. The Bragg reflections indicated at the bottom by vertical bars correspond to each of the above-mentioned phases. The presence of the $\varepsilon$-phase has been highlighted using arrows. Structural data obtained from the refinement are summarized in Table II. It is worth noting that almost all the diffractograms present a rather high background with a nontrivial dependence on $2\theta$. The reason is most probably the presence of noncrystalline Sn retained by quenching from the melt. There is also weak evidence of some LT-$\eta$-phase in very small amounts. Deeper discussion of these issues is presented in a separate report dealing with *in situ* high-temperature measurements.[24] For this reason, the Rietveld refinements present rather high values of $\chi^2$ and the data backgrounds are not perfectly accounted for. How-

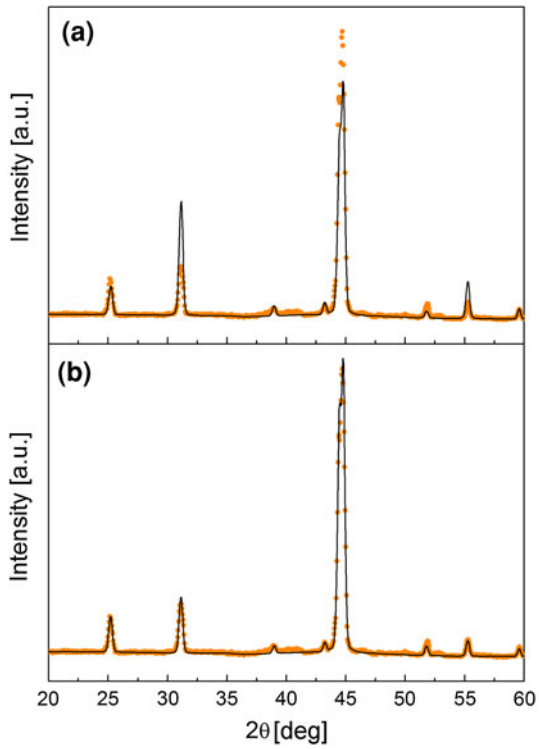


Fig. 4. (a) Best fit of the $\eta$-phase based on the model proposed in the databases, where Cu and Sn atoms occupy randomly the Wyckoff positions *2a* and *2c* of space group $P6_3/mmc$. (b) Improvement of the fit when the site occupancies correspond to the model in Fig. 3b.

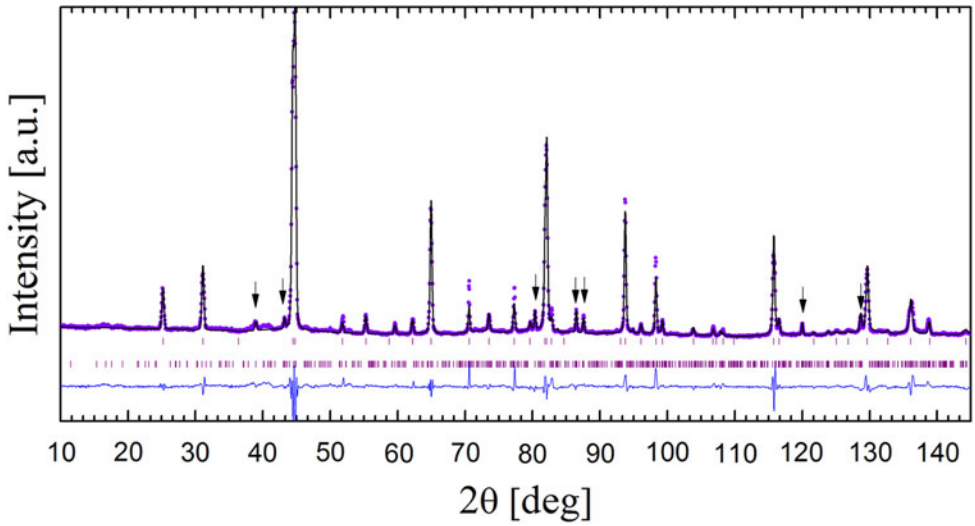


Fig. 5. Rietveld refinement for sample S1 with nominal composition 55 at.% Cu-45 at.% Sn quenched from 300°C, from ND data collected at room temperature. Vertical bars at the bottom indicate Bragg reflections from the HT-$\eta$-phase and the orthorhombic $\varepsilon$-phase. The most intense reflections from the latter have been indicated with arrows. The line at the bottom corresponds to the difference between the experimental and calculated patterns.

**Table II. Structural parameters refined from ND data at room temperature**

| | S1 | S2 | S3 | S4 | S5 | S6 | S7 |
|---|---|---|---|---|---|---|---|
| $\eta$-Phase | | | | | | | |
| $a$ | 4.2141(1) | 4.2129(1) | 4.2157(1) | 4.2187(1) | 4.2366(1) | 4.2465(1) | 4.2500(1) |
| $c$ | 5.1061(2) | 5.1045(2) | 5.1064(1) | 5.1091(1) | 5.1328(2) | 5.1607(2) | 5.1785(2) |
| $f_\eta$ | 0.95(1) | 0.98(1) | 0.99(1) | 1.00 | 0.98(2) | 1.00 | 1.00 |
| $Occ_{Cu\ -\ 2a}$ | 1.00 | *1.00* | *1.00* | *1.00* | 1.00 [1.00] | 0.95 [1.00] | 1.00 [1.00] |
| $Occ_{Cu\ -\ 2d}$ | 0.22 [0.22] | 0.20 [0.22] | 0.21 [0.22] | 0.23 [0.22] | 0.35 [0.38] | 0.43 [0.5] | 0.46 [0.5] |
| $Occ_{Sn\ -\ 2c}$ | 1.00 | 0.98 [0.98] | 0.955 [0.94] | 0.936 [0.89] | 0.77 [0.71] | 0.50 [0.5] | 0.40 [0.4] |
| $Occ_{In\ -\ 2c}$ | 0.00 | *0.02* | *0.06* | *0.11* | *0.28* | 0.47 [0.5] | 0.61 [0.6] |
| $R_B$ | 9.44 | 8.43 | 11.6 | 9.9 | 6.8 | 14.2 | 8.7 |
| $\varepsilon$-Phase | | | | | | | |
| $a$ | 5.5216(5) | 5.5230(5) | *5.5230* | – | 5.5217(8) | – | – |
| $b$ | 47.772(5) | 47.776(5) | *47.776* | – | 47.724(5) | – | – |
| $c$ | 4.3280(5) | 4.3281(5) | *4.3281* | – | 4.3302(5) | – | – |
| $f_\varepsilon$ | 0.05(1) | 0.02(1) | 0.01(1) | 0 | 0.02(2) | 0 | 0 |
| $R_B$ | 25.5 | 38.5 | – | – | 41 | – | – |
| $\chi^2$ | 18.4 | 30.0 | 16.3 | 15.1 | 9.0 | 9.9 | 8.3 |

The $\eta$-phase was refined in the $P6_3/mmc$ space group with occupied Wyckoff positions $2a = (000)$, $2c = (\frac{1}{3}\frac{2}{3}\frac{1}{4})$ and $2d = (\frac{1}{3}\frac{2}{3}\frac{3}{4})$. Only the values of refined occupancy are reported in the table. Next to the refined values, the nominal occupancies for each site using model A (see text) are indicated in brackets. Numbers in italics represent fixed parameters. The $\varepsilon$-phase was refined in the orthorhombic space group *Cmcm* after Ref. 22. Lattice parameters, phase fractions ($f$), and refined occupancies are reported, as well as indicators of the quality of the fits.

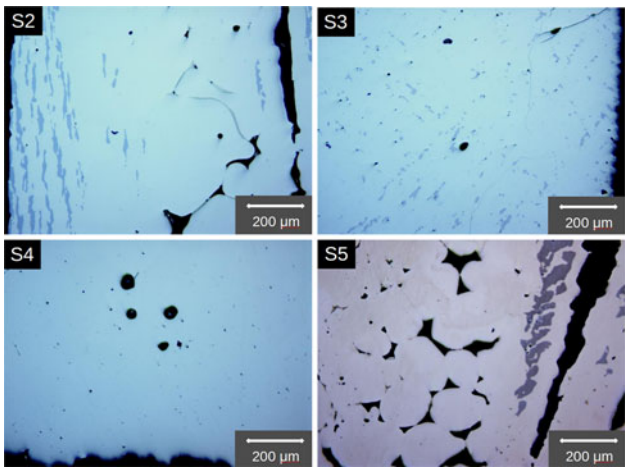


Fig. 6. Optical micrographs for samples S2–S5. The $\eta$-phase grains are well developed, and some $\varepsilon$-phase is also observed in most samples, particularly at the ingot's edges.

ever, this does not affect the most relevant structural results obtained from the fits.

The metallographies from samples with increasing In content, up to S5 (nominal 12 at.% In-30 at.% Sn), present the same trend as sample S1. They all consist mostly of a homogeneous phase (consistent with the $\eta$-phase composition), surrounded by some Sn-rich grain boundary segregation, plus some traces of a second segregated phase (consistent with the $\varepsilon$-phase composition) at the edges. This is illustrated in Fig. 6 for samples S2–S5.

Figure 7 shows the ND data for samples S5–S7. When In is added to the alloys, we can see from the diffraction data that no further reflections appear, indicating that In is indeed being incorporated into the crystal structure of $Cu_6Sn_5$. However, a further set of samples with increasing In content along the proposed $\eta$-phase field, which will be reported in a separate paper, already show the presence of additional reflections for 27 at.% In.[24] In the following we focus on samples with less than 25 at.% In.

The question now arises about the location of the In atoms in the $\eta$-phase. In the Rietveld refinement, it is not possible to set all the occupancies as free parameters given that there are three atomic species to allocate in three possible crystallographic sites, resulting in an undetermined system of equations. A second set of complementary experimental data would be needed to solve the problem. Instead, we selected, among the various possibilities, two models which are consistent with the atomic distribution in both end binaries. In model A, copper atoms completely occupy site *2a*, as was unambiguously obtained from the refinement of sample S1. Tin and indium atoms completely occupy site *2c* in proportions according to the stoichiometry of the alloy, and excess copper occupies site *2d*, which may remain partially unoccupied. In model B, site *2c* is completely occupied by tin, whereas site *2d* is shared by copper and indium

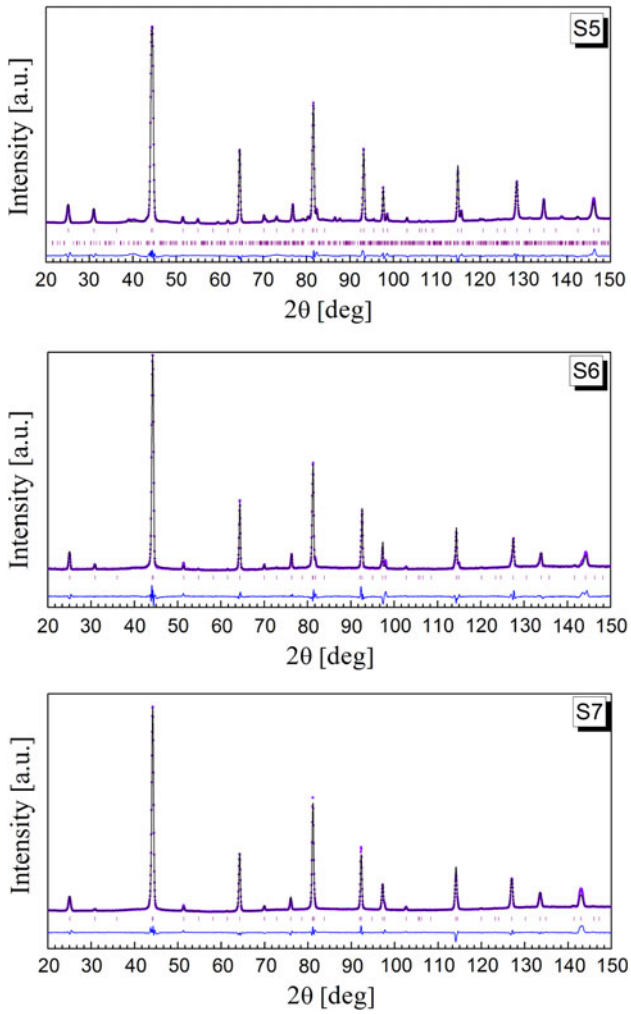


Fig. 7. Rietveld refinements for samples S5–S7 with nominal compositions 58 at.% Cu-30 at.% Sn-12 at.% In, 60 at.% Cu-20 at.% Sn-20 at.% In, and 60 at.% Cu-16 at.% Sn-24 at.% In, quenched from 300°C, from ND data collected at room temperature. Vertical bars at the bottom indicate Bragg reflections from the phases included in the refinement: the HT-$\eta$-phase and the orthorhombic $\varepsilon$-phase (just in S5). The line at the bottom indicates the difference between the experimental and calculated patterns.

atoms. Based on the above models and the nominal composition of each alloy, the occupancy at each site should be governed by the following relations:

$$\frac{1+\mathrm{Cu}(2d)}{2+\mathrm{Cu}(2d)+\mathrm{In}(2d)}38; = \text{at.\% Cu}$$

$$\frac{\mathrm{In}(2c)+\mathrm{In}(2d)}{2+\mathrm{Cu}(2d)+\mathrm{In}(2d)}38; = \text{at.\% In}$$

$$\frac{1-\mathrm{In}(2c)}{2+\mathrm{Cu}(2d)+\mathrm{In}(2d)}38; = \text{at.\% Sn},$$

where Cu(2$d$) stands for the occupancy of Cu at the 2$d$ site. For model A, we assume In(2$d$) = 0 and calculate the remaining nominal occupancies as

$$\mathrm{Cu}(2d)38; = \frac{2\times\text{at.\% Cu}-1}{1-\text{at.\% Cu}}$$

$$\mathrm{In}(2c)38; = \frac{\text{at.\% In}}{1-\text{at.\% Cu.}}$$

$$\mathrm{Sn}(2c)38; = 1-\mathrm{In}(2c)$$

For model B, we set In(2$c$) = 0 and calculate the nominal occupancies as

$$\mathrm{Cu}(2d)38; = \frac{1-2\times\text{at.\% Cu}-\text{at.\% In}}{\text{at.\% Sn}}$$

$$\mathrm{In}(2d)38; = \frac{\text{at.\% In}}{\text{at.\% Sn}}$$

$$\mathrm{Sn}(2c)38; = 1.$$

Refinements were first conducted using the above nominal occupancies as fixed parameters. The comparison did not give clear conclusions for S2, but from S3 to S7 it was clear that model B could not account for the data. In a further step, some occupancies were set as free parameters starting from model A, which resulted in the fits shown in Fig. 7. The same procedure was applied using model B, but the refined occupancies moved to values lacking physical consistency, whereas the use of model A converged to very reasonable values. In Table II we list the refined occupancies. Next to the refined values, the nominal occupancies based on model A are quoted in brackets. Occupancies in italics indicate fixed parameters.

There are certain issues to note. As stated above, only a complementary set of experimental data would allow simultaneous refinement of all the occupancies. The present model leads to good agreement with the data, but there may be other combinations that are also possible. For this reason, further experiments on the same samples are in progress to tackle this question using a site-specific technique such as synchrotron x-ray absorption fine-structure spectroscopy. Secondly, let us recall that a further hint about the probable site for In could be at the Cu-In side of the phase diagram. The literature on the binary $Cu_2In$ $\eta$-phase, however, shows severe inconsistencies. Focusing just on the hexagonal HT form of this phase, sharing the same space group as $Cu_6Sn_5$, the In atoms are reported either in the 2$c$ site (ICSD 102982 after Ref. 18, ICSD 627998 after Ref. 19) or in the 2$d$ site (ICSD 657611 after Ref. 25). The discussion above would give support to the former.

In Table II we summarize the most relevant crystallographic parameters obtained from the refinement of samples S1–S7. Although the site occupancies are constrained to the above picture, the structural parameters should not be severely affected. In the following section we discuss their composition dependence.

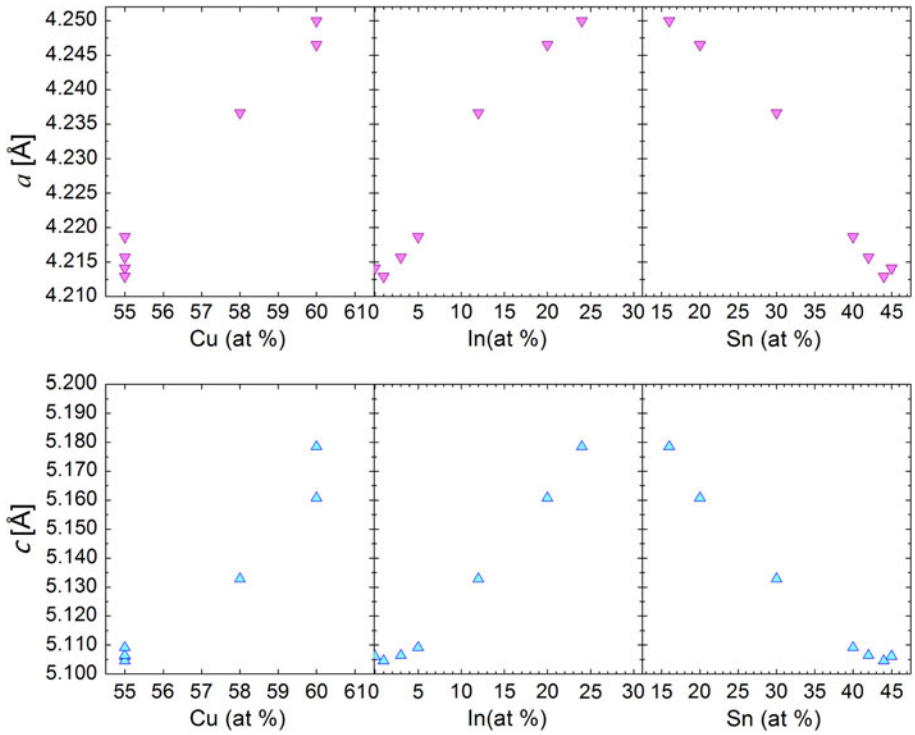


Fig. 8. Lattice parameters of the hexagonal $\eta$-phase as a function of each alloying element concentration.

## Structural Parameters as a Function of Composition

In Fig. 8 we present the lattice parameters $a$ (upper panels) and $c$ (lower panels) as a function of each component concentration. We observe that the $c$ parameter is controlled by the Cu concentration in the In-poor region, whereas for more In-concentrated alloys there is a linearity in the lattice parameters with concentration.

To rationalize the composition dependence of the $\eta$-phase volume, we present in Fig. 9 a plot of the unit cell volume as a function of the average atomic (covalent) radius, calculated as $\langle r\rangle$ [Å] = at.% Cu $\times 1.32$ Å + at.% Sn $\times$ 1.39 Å + at.% In $\times$ 1.42 Å, where the values for the individual atomic species were taken from Ref. 26. On the same graph we represent the calculated volume for data from the binaries $Cu_6Sn_5$ and $Cu_2In$. It is interesting to note that, for the first four alloys, sharing the same Cu content, the volume of the cell remains almost unchanged, and the volume is governed by the Cu fraction. Between samples S4 and S5, although they have the same average radius $\langle r\rangle$, there is a jump in volume due most probably to the doubling of the In content together with an increase in Cu from 55 at.% to 58 at.%. The alloys reported by Che and Ellner[25] for the $Cu_2In$ phase, with a Cu concentration around 66 at.%, illustrate clearly the strong dependence of volume on Cu concentration. Finally, we show in Fig. 10 the $c/a$ ratio for the present alloys, together with that reported by Che and Ellner[25] for $Cu_2In$.

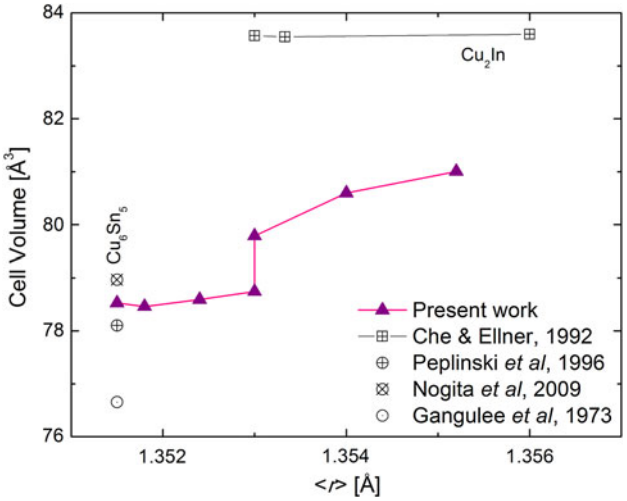


Fig. 9. Unit cell volume of the $\eta$-phase as a function of the average atomic (covalent) radius. Data for the binaries $Cu_6Sn_5$ and $Cu_2In$ from Refs. 14, 17, 20, 25 are also presented.

## CONCLUSIONS

Although much work has been devoted to the study of intermetallic phases in Cu-Sn and Cu-In alloys, a systematic diffraction study of ternary Cu-In-Sn alloys was still lacking. The present work has been devoted to study the $\eta$-phase field region in the ternary phase diagram. We present here data from neutron diffraction, a technique not used

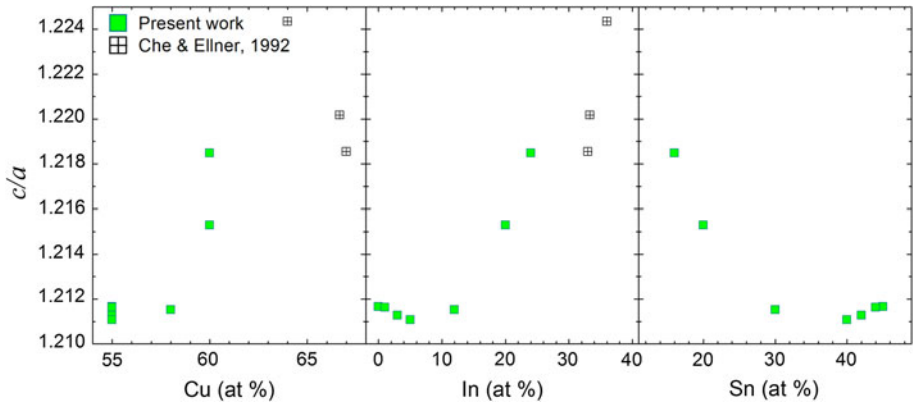


Fig. 10. Axial ratio $c/a$ for the ternary $\eta$-phase as a function of concentration of each alloying element.

before—to the best of our knowledge—to study these systems. We found this technique to be extremely useful to overcome common experimental difficulties related to XRD measurements, which may be at the origin of the confusing and inconsistent information available in the standard crystallographic databases. Our results confirm that In additions between 0 at.% and 25 at.% can stabilize the $\eta$-phase at 300°C without forming further superstructures, as proposed in the available phase diagrams.[4,6] However, further In addition results in the appearance of a number of extra, weak Bragg reflections indicating either phase coexistence or superstructure formation. Those alloys are not discussed in the present paper, and will be reported separately. A discussion has also been presented about the possible site occupancies for each element in the ternary phase. To sum up, structural data for the ternary $\eta$-phase are reported, which can be of value in the study and modeling of diffusion processes for new bonding technologies, as well as for calculations of stable and metastable phases in the ternary phase diagram.

## ACKNOWLEDGEMENTS

This work is part of a research project supported by the Agencia Nacional de Promoción Científica y Tecnológica under grant PICT2006-1947. We particularly acknowledge ILL and its staff for the beamtime allocation and technical assistance, and Dr. H. Fischer for his careful reading of the manuscript.

## REFERENCES

1. A.T. Dinsdale, A. Kroupa, J. Vízdal, J. Vrestal, A. Watson, and A. Zemanova, *COST Action 531-Atlas of Phase Diagrams for Lead-free Solders*, vol. 1 (Brussels: COST Office, 2008), p. 182.
2. W. Gale and D. Butts, *Sci. Technol. Weld. Join.* 9, 283 (2004).
3. T. Velikanova, M. Turchanin, and O. Fabrichnaya, *Cu-In-Sn (Copper-Indium-Tin)* (Stuttgart: Materials Science International Team MSIT, 2007), p. 249.
4. W. Koester, T. Goedecke,and D. Heine, *Z. Metallkd.* 63, 802 (1972).
5. S.K. Lin, C.F. Yang, S.H. Wu, and S.W. Chen, *J. Electron. Mater.* 37, 498 (2008).
6. S.K. Lin, T.Y. Chung, S.W. Chen, and C.H. Chang, *J. Mater. Res.* 24, 2628 (2009).
7. X.J. Liu, H.S. Liu, I. Ohnuma, R. Kainuma, K. Ishida, V. Itabashi, K. Kameda, and K. Yamaguchi, *J. Electron. Mater.* 30, 1093 (2001).
8. M. Elding-Pontén, L. Stenberg, and S. Lidin, *J. Alloys Compd.* 261, 162 (1997).
9. Z. Bahari, E. Dichi, B. Legendre, and J. Dugué, *Thermochim. Acta* 401, 131 (2003).
10. K.C. Jain, M. Ellner, and K. Schubert, *Z. Metallkd.* 63, 258 (1972).
11. P.R. Subramanian and D.E. Laughlin, *Bull. Alloy Phase Diagr.* 10, 554 (1989).
12. K. Nogita, *Intermetallics* 18, 145 (2010).
13. U. Schwingenschlögl, C.D. Paola, K. Nogita, and C.M. Gourlay, *Appl. Phys. Lett.* 96, 061908 (2010).
14. B. Peplinski, G. Schulz, D. Schultze, and E. Schierhornand, *Mater. Sci. Forum* 228–231, 577 (1996).
15. T.B. Massalski, *Binary Alloy Phase Diagrams*, 2nd ed. (Materials Park: ASM International, 1990).
16. J. Rodríguez-Carvajal (Abstracts of the Satellite Meeting on Powder Diffraction of the XV Congress of the IUCr, Toulouse, France, 1990), p. 127.
17. A. Gangulee, G.C. Das, and M.B. Bever, *Metall. Mater. Trans. B* 4, 2063 (1973).
18. F. Laves and H.J. Wallbaum, *Z. Anorg. Allg. Chem.* 250, 110 (1942).
19. R.S. Kalyana-Raman, R.K. Gupta, M.N. Sujir, and S. Bhan, *J. Sci. Res. Banaras Hindu Univ.* 14, 95 (1964).
20. K. Nogita, C. Gourlay, and T. Nishimura, *JOM* 61, 45 (2009).
21. K. Momma, and F. Izumi, *J. Appl. Crystallogr.* 41, 653 (2008).
22. Y. Watanabe, Y. Fujinaga, and H. Iwasaki, *Acta Crystallogr. B* 39, 306 (1983).
23. P. Brooks and E. Gillam, *Acta Metall.* 18, 1181 (1970).
24. G. Aurelio, S.A. Sommadossi, and G.J. Cuello, Neutron diffraction study of the stability and phase transitions in Cu-Sn-In alloys as alternative Pb-free solders. *J. Appl. Phys.*, submitted.
25. G.C. Che and M. Ellner, *Powder Diffr.* 7, 107 (1992).
26. B. Cordero, V. Gómez, A.E. Platero-Prats, M. Reves, J. Echeverría, E. Cremades, F. Barragan, and S. Álvarez, *Dalton Trans.* 21, 2832 (2008).